**JOURNAL OF THEORETICAL AND APPLIED MECHANICS**
**43**, 4, pp. 731-743, Warsaw 2005

# FATIGUE CRACK GROWTH RATE IN ALUMINIUM ALLOY INCLUDING MIXED MODE I AND III[1]

Dariusz Rozumek

*Faculty of Mechanical Engineering, Technical University of Opole*
*e-mail: drozumek@po.opole.pl*

The paper contains results of experimental tests on the fatigue crack growth rate of AlCuMg1 aluminium alloy for Mixed Mode I and Mode III in conditions of different stress ratios $R$. For the tests, plane specimens with an external unilateral sharp notch as the stress concentrator were used. The tests were done for a constant moment amplitude under bending with torsion. The results of experimental tests were described by a nonlinear formula based on the $\Delta J$-integral range. The change of the stress ratio $R$ from $-1$ to $0$ caused the fatigue crack growth rate. The proposed formula for description of the fatigue crack growth rate, including the $\Delta J$-integral range, satisfactorily described the results obtained experimentally for AlCuMg1 aluminium alloy.

*Key words:* fatigue crack growth, $\Delta J$-integral range, stress ratio, mixed mode

## Notations

| | | |
|---|---|---|
| $l$ | – | length of specimen |
| $g$ | – | thickness of specimen |
| $da/dN$ | – | fatigue crack growth rate |
| $\Delta J$ | – | integral range |
| CTOD | – | crack tip opening displacement |
| $R$ | – | stress ratio |
| $M_a$ | – | amplitude of the moment |
| $\sigma_u$ | – | ultimate tensile stress |

[1]This paper was presented on the 7th Conference on Biaxial/Multiaxial Fatigue and Fracture, June 2004, Berlin, Germany

$\sigma_y$ – yield strength
$\nu$ – Poisson's ratio
$K'$ – coefficient of strain cyclic hardening
$\sigma'$ – fatigue strength coefficient
$b, c$ – fatigue strength and ductility exponent, respectively

## 1. Introduction

Tests of crack mechanics are usually concentrated on the crack growth for Mode I (Rozumek, 2003). However, many failures are caused by crack growths in Mixed Modes of loading. In Qian and Fatemi (1996), we can find a review of different criteria and quantities proposed in literature for the prediction of crack growth rates in Mixed Modes I, II and III. Wasiluk and Golos (2000) presented the influence of the plastic zone near the crack tip for Mixed Modes I and II under a plane stress state. For the assumed loading state, it was proposed that the crack course proceeds in the direction in which the plastic zone radius reaches its minimum. A good agreement between the experimental data and the proposed criterion was obtained. Pook (2002) suggested that the influence of nonlinearity near the crack tip should be included in the finite element method (FEM). Calculations were performed for Modes I and II, taking into account nonlinearity near the crack tip. For Mode I, the crack tip becomes blunt. The comparison of the results from the nonlinear model (Pook, 2002) with the linear model for FEM implies small differences, and they are of no practical value. In Mode II, however, the loading behaviour is totally different. The crack tip remains sharp, and the nonlinearity occurring in the solution does not influence the obtained results. In the paper by Richard (2003), the problems of the Mixed-Mode under fatigue crack growth are dealt with. Richard 2003) presented hypotheses and concepts that describe superposition of Mode I and Mode II (plane Mixed Mode) as well as superposition of all three Modes (Mode I, II and III) for spatial loading conditions. Those concepts admit a quantitative appraisal of such crack situations and a characterisation of possible crack paths.

The aim of this paper is the experimental verification of relationships describing the fatigue crack growth rate for Mixed Mode I and III including the $\Delta J$-integral range.

## 2. Concept for determination of crack growth direction (the $\Delta J$-criterion)

For the case of Mixed-Mode (I + III) loading, we assume the $\Delta J$-integral range value. The sum of $\Delta J_{\mathrm{I}}$ and $\Delta J_{\mathrm{III}}$ will be denotes as

$$\Delta J_{\mathrm{I+III}} = \Delta J_I + \Delta J_{\mathrm{III}} \tag{2.1}$$

In the following, see Fig. 8, $\Delta J_{\mathrm{I+III}}$ is denoted as $\Delta J$ for simplicity.

The $\Delta J$-integral range for Mode I and III is expressed by following equations

$$\begin{aligned} \Delta J_I &= \frac{1-\nu^2}{E}\Delta K_I^2 + \frac{\pi Y_1^2 a}{\sqrt{n'}}\Delta\sigma\Delta\varepsilon_p \\ \Delta J_{\mathrm{III}} &= \frac{1+\nu}{E}\Delta K_{\mathrm{III}}^2 + \frac{\pi Y_3^2 a}{\sqrt{n'}}\Delta\tau\Delta\gamma_p \end{aligned} \tag{2.2}$$

where $a$ is the crack length, $E$ – Young's modulus, $\Delta\sigma$, $\Delta\tau$ – stress ranges under bending and torsion at the root of the notch, respectively, $\Delta\varepsilon_p$, $\Delta\gamma_p$ – plastic strain ranges under bending and torsion at the root of the notch, respectively, $n'$ – cyclic strain hardening exponent.

The range of stress intensity factors for Mode $\Delta K_{\mathrm{I}}$ and Mode $\Delta K_{\mathrm{III}}$ have the form

$$\begin{aligned} \Delta K_I &= Y_1\sqrt{\pi a}\Delta\sigma\cos^2\alpha \\ \Delta K_{\mathrm{III}} &= Y_3\sqrt{\pi a}\Delta\sigma\sin\alpha\cos\alpha \end{aligned} \tag{2.3}$$

and for Mode I and III, according to Harris (1967) and Chell and Girvan (1978), the correction coefficients take the forms

$$Y_1 = \frac{5}{\sqrt{20 - 13\frac{a}{w} - 7\left(\frac{a}{w}\right)^2}} \qquad Y_3 = \sqrt{\frac{2w}{a}\tan\frac{\pi a}{2w}} \tag{2.4}$$

where $w$ is height of a specimen.

The test results presented in the paper for description of ranges II and III of crack growth kinetics were approximated by the following empirical formula (Rozumek, 2003)

$$\frac{da}{dN} = \frac{B\left(\frac{\Delta J}{J_0}\right)^n}{(1-R)^2 J_{\mathrm{Ic}} - \Delta J} \tag{2.5}$$

where $J_{Ic}$ is the critical value of the $J$ integral, $\Delta J = J_{max} - J_{min}$. $J_0 = 1\,\text{MPa·m}$ – per unit is a value introduced to simplify the coefficient unit $B$, $B$ and $n$ are coefficients and exponents determined experimentally.

## 3. Materials and test procedure

Plane notched specimens made of AlCuMg1 aluminium alloy were tested (Fig. 1). The specimens were made of a drawn bar 16 mm in diameter.

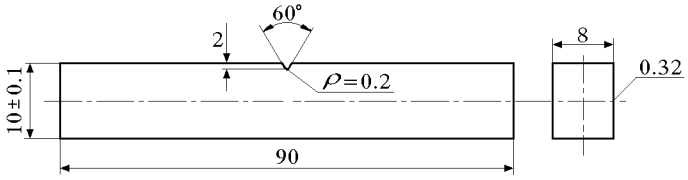


Fig. 1. Shape and dimensions of a notched specimen

The specimens had an external, unilateral notch which was 2 mm deep. Their radius was $\rho = 0.2\,\text{mm}$. The notches were made by milling and the surface of the specimens was ground. The theoretical stress concentration factor in the specimen under bending $K_{tB} = 3.76$, was estimated with use of the model by Thum *et al.* (1960). Its chemical composition and mechanical properties are given in Tables 1 and 2. Table 3 contains some cyclic properties of the material. The results of the tests presented in Tables 1, 2 and 3 were obtained at the Technical University of Opole.

**Table 1.** Chemical composition of the aluminium alloy [%]

| Cu | Mn | Zn | Mg | Fe | Cr | Si | Ti |
|---|---|---|---|---|---|---|---|
| 4.15 | 0.65 | 0.50 | 0.69 | 0.70 | 0.10 | 0.45 | 0.20 |

**Table 2.** Mechanical properties of the aluminium alloy

| $\sigma_y$ [MPa] | $\sigma_u$ [MPa] | $E$ [GPa] | $\nu$ | $J_{Ic}$ [MPa·m] |
|---|---|---|---|---|
| 382 | 480 | 72 | 0.32 | 0.026 |

**Table 3.** Cyclic properties of the aluminum alloy

| $K'$ [MPa] | $n'$ | $\sigma'_f$ [MPa] | $b$ | $c$ |
|---|---|---|---|---|
| 563 | 0.033 | 605 | −0.051 | −0.858 |

The tests were done on the fatigue test stand MZGS-100 (Achtelik and Jamroz, 1982), see Fig. 2, enabling realisation of cyclic loading with a mean value inducing plane stress on the material surface. The propagating crack length was measured with an optical device including a digital micrometer and a microscopic telescope magnifying 25-times. The fatigue crack length was periodically measured after each thousand of cycles with accuracy not less than 0.01 mm. Unilaterally restrained specimens were subjected to cyclic bending with torsion at the amplitude moment $M_a = 7.92\,\mathrm{N{\cdot}m}$ ($M_a$ is for combined bending and torsion). The stress ratio range was $R = \sigma_{min}/\sigma_{max} = -1.0$, $-0.5$, 0.0, respectively. The specimen loading included static and cyclically variable forces. Mixed Mode I and III were obtained by rotation of head 2 (Fig. 2a) by angle $\alpha$, as shown in Fig. 2b. For the angle $\alpha = 0^\circ$, pure pure bending is obtained, whereas for $\alpha = 90^\circ$ one gets pure torsion. In Fig. 2b, $M(t)$ is the ratio of torsional and bending moments $M_T(t)/M_B(t) = tan\alpha = \sqrt{3}/3$. The total moment $M(t) = 2\sqrt{3}M_B(t)/3$ was caused by a force applied to the arm of 0.2 m in length.

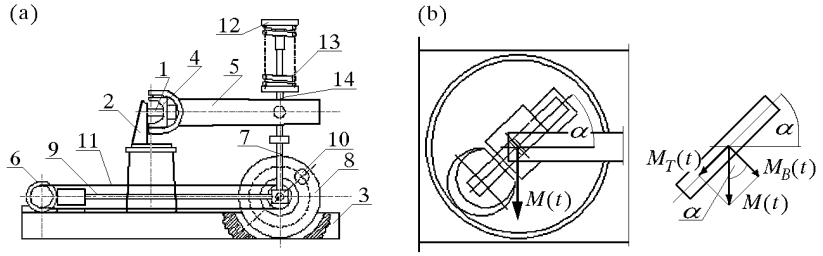


Fig. 2. Fatigue test stand MZGS-100 (a) and loading of the specimen (b) where: 1 – specimen, 2 – rotational head with a holder, 3 – bed, 4 – holder, 5 – lever (effective length = 0.2 m), 6 – motor, 7 – lower string, 8 – rotating disk, 9 – flat springs, 10 – unbalanced mass, 11 – driving belt, 12 – spring actuator, 13 – spring, 14 – upper string

The specimens shown in Fig. 2b were tested under proportional bending with torsion and stresses coming from the bending and torsion occurred during the tests. Normal stresses came from bending and they changed from zero in the neutral layer to the maximum value in the notch root (extreme fibres) of the specimen. Torsion caused shear stresses changing from zero in the specimen axis to the maximum value in the farthest points from the specimen axis (in the center of the square sides). For specimens with the square (rectangular) section, their cross sections were subjected to deformation or the so-called deplanation during torsion. If torsion was unfree (as in the presented case), there appeared two kinds of stresses: shear stresses plus normal stresses from

torsion itself. During crack initiation and in the notch influence period (in the bending plane up to about 2 mm), the stresses caused by bending were about 2.7 times greater than those caused by torsion. The specimen shape shown in Fig. 2b allowed one to observe and measure crack development during the whole process of fatigue tests.

### 3.1. Numerical method

The $J$-integrals were calculated with the finite element method (FEM) with the help of the program FRANC2D in the whole test range as well as with the boundary element method (BEM) supported by the program FRANC3D in the linearly elastic range in order to compare the influence of thickness for that type of specimens. Having made the specimen outline, segments were divided and closed areas were defined (Rozumek and Lewandowski, 2004). A finite (boundary) element network was put on each area. The program designs the network automatically. Figure 3 shows the division of the notch region into boundary elements.

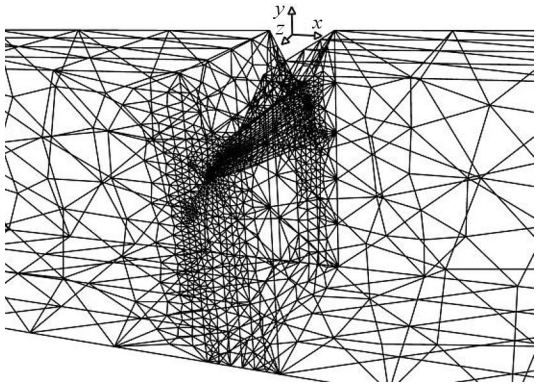


Fig. 3. Division of the notch region into finite elements in the program FRANC3D and crack growth in the notch

In the model presented in Fig. 3, ten-nodal tetrahedron elements were used. For calculations, the same loading values as those used in the experiments were assumed. The magnitude and shape of boundary elements depend on the division of intervals closing a given area. The greatest network concentration occurs in the area of crack development (Fig. 3). Next, one end of the specimen is restrained (thus taking away degrees of freedom from the nodes of the specimen model) and it is fixed in the direction of axes $x$, $y$ and $z$. In order to perform numerical calculations, it is necessary to introduce material data (such as the yield point, Young's modulus, Poisson's ratio, temperature,

material density, critical value – for example, $J_{Ic}$ integral) into the FRANC3D program. It is also possible to introduce a variant of the material work range, for example elastic, plastic and so on. After introducing these data, it is necessary to define the loading. Since it is not possible to introduce the loading torque directly, it is replaced by a pair of forces acting on an arm and applied to the nodes. The forces (moments) load the specimen model in the same way as during the experiments, i.e. the model arm is increased so as the occurring shearing force could be neglected (in the experiments the value of this force was less than 2% of total stress). After simultaneous application of the bending and torsion moments, calculations began.

Calculations were done with the incremental method for crack lengths which were obtained in the tests for further comparison. Exemplary results of numerical calculations are shown in Fig. 4 – Fig. 6 as maps of normal stresses along the $x$ axis (active and passive side) and shear stresses along the $xy$ axes as well as the crack tip opening displacement (CTOD). Non-uniform increment of the crack length on both sides of the specimens, i.e. at the front and at the back, was found (as in the experiments). It was found that there was some influence of the specimen thickness (plane strain). The relative error of the compared methods was below 16%. The cyclic strain curve based on the nonlinear material model was introduced into the program FRANC2D. In that case, the cyclic strain curve for AlCuMg1 aluminium alloy described by the Ramberg-Osgood relation was used.

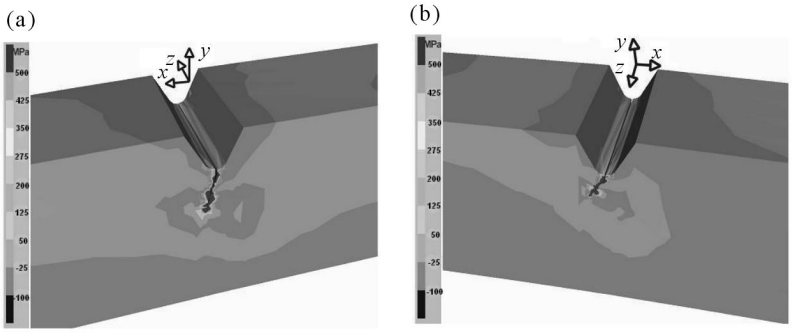


Fig. 4. Normal stress distribution along the $x$ axis under total loading with the moment coming from bending with torsion $M_a = 7.92\,\mathrm{N{\cdot}m}$ ($R = -1$) and the crack length $a = 2.15\,\mathrm{mm}$, (a) active side, (b) passive side

The introduced curve was the basis for calculations of stresses, strains, $J$-integrals and CTOD. The calculations were performed for two-dimensional and three-dimensional geometrical models of notched specimens.

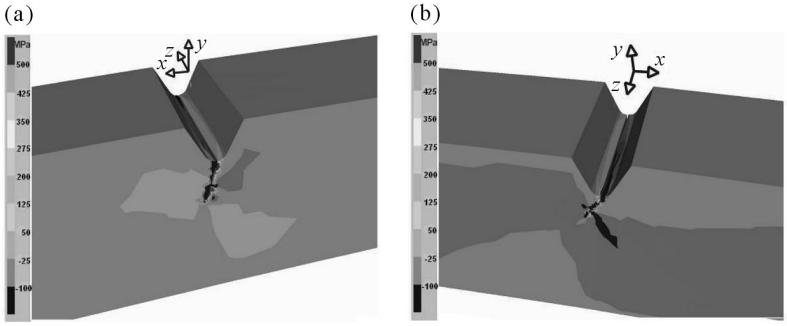


Fig. 5. Shear stress distribution along the $x$ axis under total loading with the moment coming from bending with torsion $M_a = 7.92\,\mathrm{N{\cdot}m}$ $(R = -1)$ and the crack length $a = 2.15\,\mathrm{mm}$, (a) active side, (b) passive side

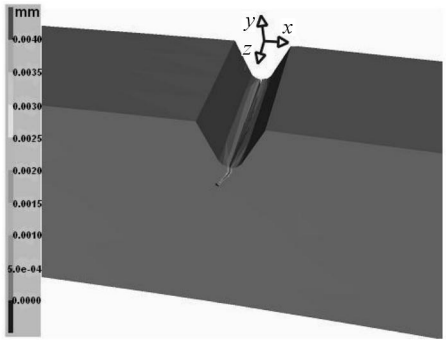


Fig. 6. Crack tip opening displacement (CTOD = 0.004 mm) under loading $M_a = 7.92\,\mathrm{N{\cdot}m}$ $(R = -1)$

## 4. Experimental results

The paper contains test results illustrating phenomena occurring in the AlCuMg1 aluminium alloy subject to fatigue cracking in Mixed Mode I and III under different stress ratios $R$. The tests were done under a controlled loading from the crack initiation to specimen failure. During tests of proportional bending with torsion, the cracks developed in a similar way as shown in Figs 3, 4 and 5 in the boundary element method. Non-uniform increment of the fatigue crack length was observed on both sides of the specimens, as in the numerical method. In the active part (loaded), the crack lengths were a little bigger than those in the passive side (unloaded). In the calculations, crack lengths were assumed for the active part because they had the main influence on the specimen failure. Measurements were done from the moment of crack

occurrence up to the specimen failure, as presented in Fig. 7 (crack lengths $a$ versus the number of cycles to failure $N$).

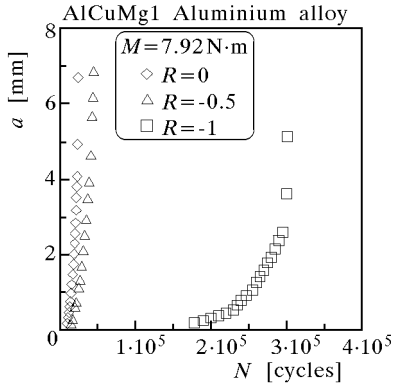


Fig. 7. Fatigue crack length $a$ versus number of cycles $N$ under combined bending and torsion

Elasto-plastic stresses and strains in Eqs. (2.2) were calculated with the finite element method and the programs FRANC2D and 3D. The test results were presented as graphs of the crack growth rate $da/dN$ versus the $\Delta J$-integral range (see Fig. 8). The tests were done at a constant loading amplitude $M_a$.

The relations between $da/dN$ and $\Delta J$ for Mode I and III were shown in Fig. 8. The crack propagation rate was expressed as a function of the $\Delta J$-integral range for pure Mode I and pure Mode III, though the results were obtained for combined bending with torsion. Direct determination of the mixed $J$-integral is impossible. From graph courses in Fig. 8, it appears that the change of the stress ratio from $-1$ to $0$ is followed by the increase in fatigue crack growth rate for Mode I and III. Moreover (Fig. 8), it was observed that the propagation rate is higher for Mode III than Mode I at the same value of the $\Delta J$-integral range. The material coefficients $B$ and $n$, occurring in Eq. (2.5), were determined with the least square method, and are presented in Fig. 8. The coefficients $B$ and $n$, which should be material constants, are in practice dependent on other factors, for example the stress ratio $R$. The maximum relative error of the presented test results did not exceed 10% for correlation at the significance level $\alpha = 0.05$ equal to $r$ from 0.98 to 0.99 and the stress ratios from $-1$ to $0$ (except for the final crack growth range for $R = 0$, where the relative error was about 22% for $r = 0.92$ – Mode III and $r = 0.91$ – Mode I). Equation (2.5) gave satisfactory results for the description of the tests.

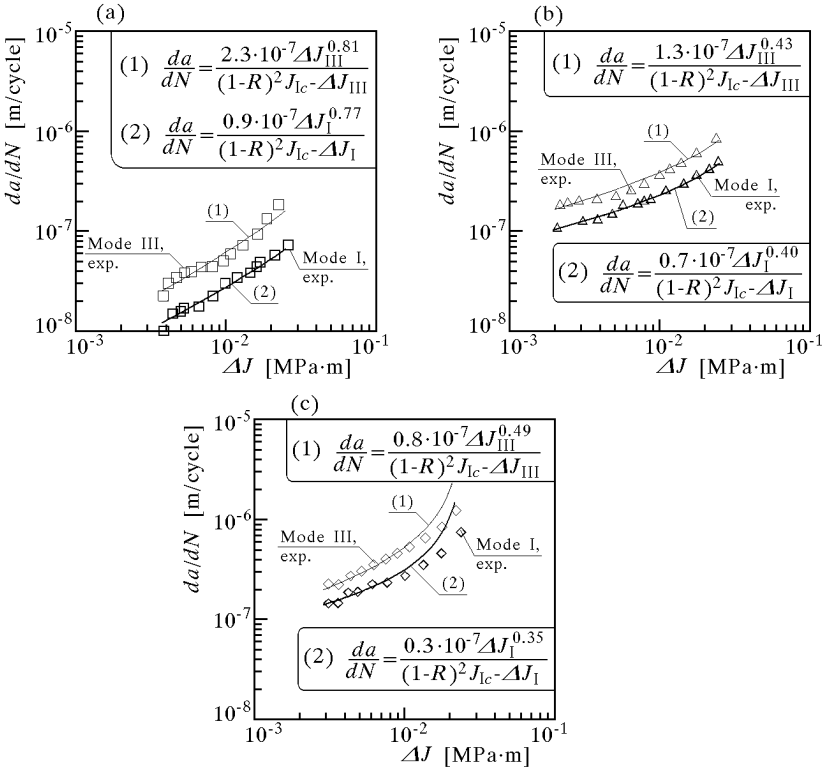


Fig. 8. Comparison of results from Eq. (2.5) with experimental results, see Eqs. (2.2) for $R=-1$ (a), $R=-0.5$ (b), $R=0$ (c) (1 – Mode III, 2 – Mode I, Eq. (2.5))

Application of the $\Delta J$ parameter is reasonable if one deals with elasto-plastic materials and materials with a visible yield point. In order to show that the application of the $\Delta J$-integral range is right, correlation between the parameters $\Delta K$ and $\Delta J$ for Mode I and Mode III has been analysed.

For this purpose, a well-known relation was used

$$\Delta J_{\mathrm{I}}^{*}=(1-\nu^2)\frac{\Delta K_{\mathrm{I}}^2}{E} \qquad \Delta J_{\mathrm{III}}^{*}=(1+\nu)\frac{\Delta K_{\mathrm{III}}^2}{E} \tag{4.1}$$

Figures 9a,b show a relationship between $\Delta J^{*}$ and $\Delta J$ for different stress ratios $R$. A good linear relationship (in a double logarithmic system) between the parameters $\Delta J^{*}$ and $\Delta J$ has been found in the case of increase of the fatigue crack growth rate in the material tested. In Mode I, it occurred for $\Delta J < 5\cdot10^{-3}$ MPa·m (Fig. 9a) and in Mode III for $\Delta J < 4\cdot10^{-3}$ MPa·m (Fig. 9b). It means that in these tests the parameter $\Delta J$ plays a similar role as $\Delta K$ up to the occurrence of plastic strains. With the increase of the plastic

strain, it has been found that the difference between $\Delta J^*$ and $\Delta J$ grows (see Fig. 9). This difference results from the fact that the parameter $\Delta J^*$ does not include plastic strains.

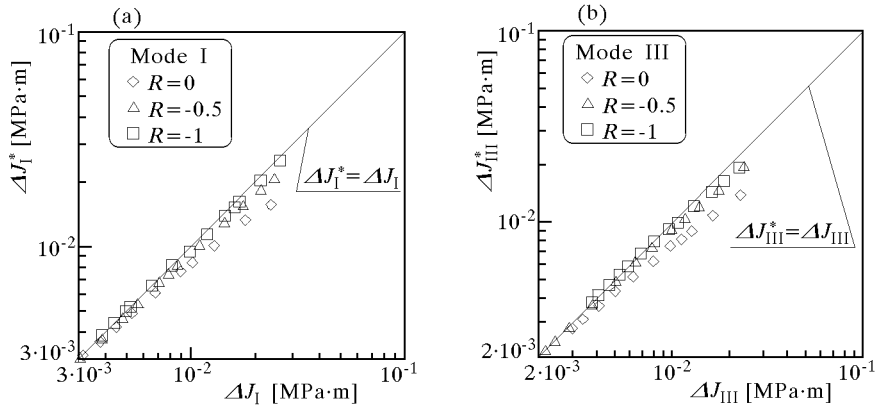


Fig. 9. Relationship between $\Delta J^*$ and $\Delta J$ for Mode I (a) and for Mode III (b)

## 5. Conclusions

The analysis of the test results leads to the following conclusions:

- The applied empirical formula, (2.5), including the $\Delta J$-integral range under Mixed-Mode I and III gives satisfactory results for the description of tests on the fatigue crack growth rate in the tested aluminum alloy.
- It has been shown that the application of the $\Delta J_{\mathrm{I(III)}}$ parameter, as compared with $\Delta K_{\mathrm{I(III)}}$, is valid for the description of the crack growth rate in the tested material.
- It has been proved that the change of the stress ratio from $R = -1$ to $R = 0$ causes increase in the fatigue crack rate.

*Acknowledgements*

This work was supported by the Commission of the European Communities under the FP5, GROWTH Programme, contract No. G1MA-CT-2002-04058 (CESTI).

## References


1. ROZUMEK D., 2003, Fatigue crack growth of notched members under bending for different stress ratios, *Materials Engineering*, **10**, 1-8
2. QIAN J., FATEMI A., 1996, Mixed mode fatigue crack growth, a literature survey, *Eng. Fracture Mechanics*, **55**, 969-990
3. WASILUK B., GOLOS K., 2000, Prediction of crack growth direction under plane stress for Mixed-Mode I and II loading, *Fatigue Fract. Eng. Mater. Struct.*, **38**, 381-386
4. POOK L.P., 2002, Linear and geometric nonlinear finite element analysis of cracked square plates under Mode I and Mode II loading, *14th European Conference on Fracture*, **II**, 695-702
5. RICHARD H.A., 2003, Theoretical crack path determination, *Int. Conf. on Fatigue Crack Paths (FCP 2003)*, Parma, CD-ROM, 15 ps
6. HARRIS D.O., 1967, Stress intensity factors for hollow circumferentially notched round bars, *J. Bas. Engng.*, **89**
7. CHELL G.G., GIRVAN E., 1978, An experimental technique for fast fracture testing in Mixed Mode, *Int. J. Fracture*, **14**, R81-R84
8. THUM A., PETERSEN C., SWENSON O., 1960, *Verformung, Spannung und Kerbwirkung*, VDI, Duesseldorf
9. ACHTELIK H., JAMROZ L., 1982, Patent PRL No.112497, CSR No.200236 and HDR No.136544, Warsaw (in Polish)
10. ROZUMEK D., LEWANDOWSKI J., 2004, Stress and strain states in square specimens under bending and combined bending with torsion for 18G2A steel, *Report*, **5** (in Polish)


## Prędkość wzrostu pęknięć zmęczeniowych w stopie aluminium przy udziale mieszanych sposobów obciążenia I i III


Streszczenie

W pracy przedstawiono wyniki badań doświadczalnych wzrostu prędkości pęknięć zmęczeniowych dla mieszanego I i III sposobu obciążenia w stopie aluminium AlCuMgl (PA6) i różnych wartości współczynnika asymetrii cyklu $R$. Do badań użyto próbek płaskich z koncentratorem naprężeń w postaci zewnętrznego jednostronnego karbu ostrego. Badania prowadzono dla stałej amplitudy momentu przy kombinacji

zginania ze skręcaniem. Wyniki badań doświadczalnych opisano nieliniowym związkiem zawierającym zakres całki $\Delta J$. Przeprowadzone badania doświadczalne potwierdziły, że zmiana współczynnika asymetrii cyklu $R$ od $-1$ do $0$ powodowała wzrost prędkości pęknięć zmęczeniowych. Zaproponowany związek do opisu prędkości wzrostu pęknięć zmęczeniowych, zawierający zakres całki $\Delta J$, w sposób zadawalający opisuje wyniki uzyskane doświadczalnie dla stopu aluminium AlCuMg1.

*Manuscript received September 30, 2004; accepted for print March 17, 2005*